

Shearing Invariant Texture Descriptor from a Local Binary Pattern and its Application in Paper Fingerprinting

Omar Wahdan, Mohammad Nasrudin, and Khairuddin Omar

Faculty of Information Science and Technology, Universiti Kebangsaan Malaysia, Malaysia

Abstract: *In this paper, a Shearing Invariant Texture Descriptor (SITD) is proposed, which is a theoretically and computationally simple method based on the Rotation invariant Local Binary Pattern (Rot-LBP) descriptor. In real-world applications using flatbed scanners, such as paper texture fingerprinting, it's common for a sheet of paper to rotate during the image acquisition process. Because the rotation is usually not based on the paper's geometrical centre pivot, the produced image is deformed with irregular rotation resulting in shearing transforms. To tackle the shearing problem, the proposed SITD selects a few patterns from the conventional Rot-LBP to achieve either horizontal or vertical invariance. This paper presents the construction of the SITD operators and their performance in recognizing self-developed and standard image datasets, including real paper texture and Outex images, as well as those with distinctive shapes. The images were distorted with only a shearing transform. The self-developed images were distorted manually, while the standard images were distorted by software. The proposed description method achieved up to 100% correctly recognition rate in all the tested datasets based on the horizontal shear invariant operator. In addition to the accurate performance in all the conducted experiments, the operator significantly outperformed the Rot-LBP and another benchmark method, the Shearing Moment Invariant (SMI). The superiority of the descriptor in recognizing different types of patterns demonstrate its ability to be used in applications where the shearing transform is present.*

Keywords: *Shear invariant descriptor, texture fingerprint, image acquisition, local binary pattern, outex framework.*

Received September 6, 2014; accepted February 4, 2015

1. Introduction

Texture image acquisition is one of the most important stages in any texture recognition application. The ultimate objective of this stage is to create a digital image from the physical scene. Traditionally, two image acquisition methods are available [5]. The first uses a movable sensor such as a microscopic digital camera or a high-powered laser, while the second uses a non-movable sensor such as a normal flatbed scanner [10]. In terms of cost and availability, the first method usually involves sophisticated, specialized, and expensive devices that are not normally available to the public. Conversely, the second method is more widely used, as ordinary flatbed scanners are cheap and broadly available [26].

The major problem with any flatbed scanning method is deformation. An ordinary scanner using a manual or automatic paper feed may turn the paper slightly during the feeding process, i.e., if the paper is scanned twice, it's cannot guarantee that the second scanned image will be exactly the same as the first [3]. In fact, this causes the captured texture to differ when the image is registered and subsequently queried [14].

A straightforward solution to match the registered and queried images is the use of any affine invariant image descriptor. Ideally, the descriptor should be invariant to any translation, scale, rotation, or shear

deformation of the image. A slight turn of the scanned paper should not naturally change the descriptor.

However, a recent investigation of deformation by scanners documented in [14] stated that, a slight rotation during the feeding process produces a shear deformation and not a normal rotation. Furthermore, it was found that the use of an affine invariant descriptor such as the Moment Invariants (MI) is not the best solution to the problem. Although, the MI descriptor covers shear variation, it is too general and prone to noise [29].

This paper proposes a new descriptor that is invariant in terms of shear variation and works well with any texture capturing application that uses an ordinary flatbed scanner. The proposed method is based on the state-of-the-art Rotation invariant descriptor, the Local Binary Pattern (Rot-LBP). The Rot-LBP is selected from many other rotation invariant descriptors based on the critical study documented in section 2. The construction of the new descriptor is defined and explained in section 3.

For the purpose of performance evaluation, the proposed shear invariant descriptor is tested using two different evaluations. First, it's challenged in a real-world problem application, namely, scanned paper texture fingerprinting. In fact, this application has attracted much attention in recent years owing to the

wide spectrum of possible domains that benefit from it. Paper fingerprinting can be used to authenticate valuable artworks or manuscripts, currency, lottery tickets, sports tickets, legal deeds, passports, certificates, and product packaging, amongst others [3, 4]. Section 4 provides an extensive explanation of the paper fingerprinting process and the obtained results.

Contrary to the naturally occurring shear deformation in images used in the first evaluation, images in the second evaluation were sheared artificially by software. The evaluation includes conducting two main experiments. The first used all 320 texture images currently available in the Outex framework [17], while the second experiment involved the 12 standard images used in the experiment presented in [14]. The results obtained from both experiments are excellent and presented in details in section 5.

In both evaluations, the chi-squared distance method is computed for feature matching. The chi-square test is well-known efficient statistical tool uses to calculate the dissimilarity of histograms (feature vectors) [15]. In both evaluations, the proposed description method is compared with the conventional Rot-LBP and Shearing Moment Invariant (SMI) descriptors. SMI is currently the sole shear-only invariant descriptor available [21].

In section 6, the conclusions and the possible real-world applications may benefit from the proposed descriptor are presented.

2. Related Works and Literature Review

Developing a successful and practical shear descriptor to handle shear variation in real-world applications using scanners for image acquisition requires knowledge about existing rotation and shear invariant descriptors. This is because shear deformation is caused by a slight rotation during paper scanning. Furthermore, as the developed shear descriptor is intended for use in real scanned paper texture fingerprinting systems, it's important to review existing texture fingerprinting methods and their limitations. The proposed descriptor should not, however, be confused with the shear let transform proposed by Guo *et al.* [6]. Contrary to the proposed method, which aims to extract features invariant against shearing deformation, the shear let system uses shear transformation and a few other morphological operations to smooth the images [24].

2.1. Rotation Invariant Texture Descriptors

Because the primary focus of this paper is on texture recognition, the existing methods in this area are broadly categorized into: structural, spectral, and statistical [12]. The structural (perceptual) approaches usually describe texture based on some properties of its textons (primitive patterns of texture) such as average texton intensity, area, perimeter, eccentricity, orientation, elongation, magnitude, and compactness

[27]. Therefore, the methods in this category require texture with regular textons. In fact, this factor may limit the possible application benefits from structural descriptors because most natural textures are irregular [19].

The spectral (frequency) approaches are based on an analysis of the power spectral density function [11]. This category includes the Rotation Invariant Simultaneous Autoregressive model (RISAR) [1], Gabor filter [8], wavelet transform [25], and Markov model [22]. However, these methods may not be suitable for adoption in developing a shearing invariant descriptor, as use of the RISAR and Gabor filter techniques is restricted by the setup of appropriate parameters for each specific application. In addition, the wavelet transforms works ideally with textures consisting primarily of smooth components, and again, natural textures are usually rough. Moreover, the local pixel neighbourhood methods based on the Varma and Zisserman (VZ) method proposed by Varma and Zisserman [23] and, from a statistical perspective, the Rot-LBP proposed by Ojala *et al.* [18] firmly place the Markov model back on the map in terms of overall performance accuracy. However, the drawback of the VZ method is its high computational cost, whereas the Rot-LBP is a simple, yet efficient rotation invariant texture descriptor [27]. Another advantage of the Rot-LBP method is its tendency to simplify the local image structure, as well as its conciseness and low computational cost [7, 18].

2.2. Shearing Moment Invariant

Prior to Shamsuddin's research [21], extracting invariant features from images distorted by shear transforms had never been discussed. Shamsuddin's proposed SMI approach as an enhanced version of the traditional well-known Hu's MI method. The SMI achieves shearing invariance by considering the following moment:

$$\eta_{pq} = \mu_{pq} \mu_{00}^{i+1} / \mu_{p+i,0} \mu_{0,q+i} \quad p, q, i = 0, 1, 2, 3, \dots \quad (1)$$

Equation 1 can be used to form the following seven shear invariant descriptors:

$$\begin{aligned} I_1 &= \eta_{20} + \eta_{02} \\ I_2 &= (\eta_{20} - \eta_{02})^2 + (4\eta_{11})^2 \\ I_3 &= (\eta_{30} - 3\eta_{12})^2 + (3\eta_{21} - \eta_{03})^2 \\ I_4 &= (\eta_{30} - \eta_{12})^2 + (\eta_{21} - \eta_{03})^2 \\ I_5 &= (\eta_{30} - 3\eta_{12})(\eta_{30} + \eta_{12})[(\eta_{30} + \eta_{12})^2 - 3(\eta_{21} + \eta_{03})^2] \\ &\quad + (3\eta_{21} - \eta_{03})(\eta_{21} + \eta_{03})[3(\eta_{30} + \eta_{12})^2 - (\eta_{21} + \eta_{03})^2] \\ I_6 &= (\eta_{20} - \eta_{02})(\eta_{30} + \eta_{12})^2 - (\eta_{21} + \eta_{03})^2 \\ &\quad + 4\eta_{11}(\eta_{30} + \eta_{12})(\eta_{21} + \eta_{03}) \\ I_7 &= (3\eta_{21} - \eta_{03})(\eta_{30} + \eta_{12})[(\eta_{30} + \eta_{12})^2 - 3(\eta_{21} + \eta_{03})^2] \\ &\quad - (\eta_{30} - 3\eta_{12})(\eta_{21} + \eta_{03})[3(\eta_{30} + \eta_{12})^2 - (\eta_{21} + \eta_{03})^2] \end{aligned}$$

However, having used the SMI descriptor in various experiments and compared it with the MI descriptor in [14], it was concluded that, even though the SMI method usually performed better than the MI one for sheared images, it could not produce near-perfect accuracy. Thus, it would be worthwhile to create a new descriptor for shear-only deformation.

2.3. Existing Texture Fingerprinting Methods

During the last decade, owing to the wide variety of possible applications, texture fingerprinting has attracted a great deal of attention. The first few applications in this area adopted expensive, movable sensor, texture acquisition devices such as microscopic digital cameras (for example, the work performed in [13, 28]) or high-powered lasers (such as those proposed by Buchanan *et al.* [2]). To avoid any affine transformations, these systems used registration marks to guide the acquisition devices.

Subsequent systems in this area adopted commodity flatbed scanners to reduce the hardware cost [3]. The difficulty with non-movable sensor acquisition devices is the natural slight rotation of sheets of paper during the paper scanning process. Furthermore, using registration marks is not a good solution because these marks cannot be used to adjust the scanner while capturing textures regardless of the effect of rotation. However, all the above-mentioned systems that used non-movable sensors arbitrarily ignored deformation effects.

3. Rotation Invariant LBP

3.1. Brief Review of Rot-LBP Theory

The Rot-LBP texture descriptor was originally introduced by Ojala *et al.* [18]. This descriptor tends to simplify the local image structure. The computation of Rot-LBP involves thresholding the grey value of each centre pixel with those of its neighbours as shown in Figure 1:

$$LBP_{P,R} = \sum_{p=0}^{P-1} s(g_p - g_c) 2^p, s(x) = \begin{cases} 1 & x \geq 0 \\ 0 & x < 0 \end{cases} \quad (2)$$

Where g is the grey value of the centre pixel, g_p is the grey value of neighbour p , P is the number of neighbours, and R is the neighbourhood radius. The $LBP_{P,R}$ assumes that $(0, 0)$ is the coordinate of g_c , while the neighbours' coordinates are $(R \cos(2\pi p/P), R \sin(2\pi p/P))$.

125	99	137
106	117	113
165	119	153

a) a 3x3 pattern

1	0	1
0	gc	0
1	1	1

b) The neighbours' values after thresholding.

Figure 1. Thresholding process based on the grey value of the centre pixel.

After calculating the $LBP_{P,R}$ value, the uniform (U) value of the pattern is obtained as:

$$U(LBP_{P,R}) = |s(g_{p-1} - g_c) - s(g_0 - g_c)| + \sum_{p=1}^{P-1} |s(g_p - g_c) - s(g_{p-1} - g_c)| \quad (3)$$

The pattern is called uniform if it's contains at most two bitwise transitions from 0 to 1 or vice versa when the corresponding bit string is considered circular. The uniform LBP ($LBP_{P,R}^{u,2}$) have been developed to reduce the complexity. This employed by reducing the number of allowed patterns of the LBP , which brings the $LBP_{P,R}^{u,2}$ to linear order.

The mapping from $LBP_{P,R}$ to $LBP_{P,R}^{u,2}$ as $P*(P-1)+3$ output values (histogram bins); these values are implemented with a 2^P element lookup table.

Local patterns can be used to achieve a rotation invariant. The Rot-LBP ($LBP_{P,R}^{riu,2}$) is given by:

$$LBP_{P,R}^{riu,2} = \begin{cases} \sum_{p=0}^{P-1} s(g_p - g_c) & \text{if } U(LBP_{P,R}) \leq 2 \\ P & \text{otherwise} \end{cases} \quad (4)$$

The mapping from $LBP_{P,R}$ to $LBP_{P,R}^{riu,2}$ has $P+2$ output values (histogram bins); these values are also implemented with a 2^P element lookup table.

Obviously, the fundamental theory behind $LBP_{P,R}^{riu,2}$ is to categorize the 2^P patterns into $P+2$ unique groups, where each group includes patterns with the same number of 1's (or 0's) in their equivalent binary numbers obtained by Equation 2. For example, the patterns 1, 2, 4, and 8 in Figure 2 have the same number of 1's (highlighted in black) in their equivalent binary numbers. By grouping these four patterns into one group, rotation invariance is achieved because the group contains all possible shapes that could occur by rotating any pattern within the group.

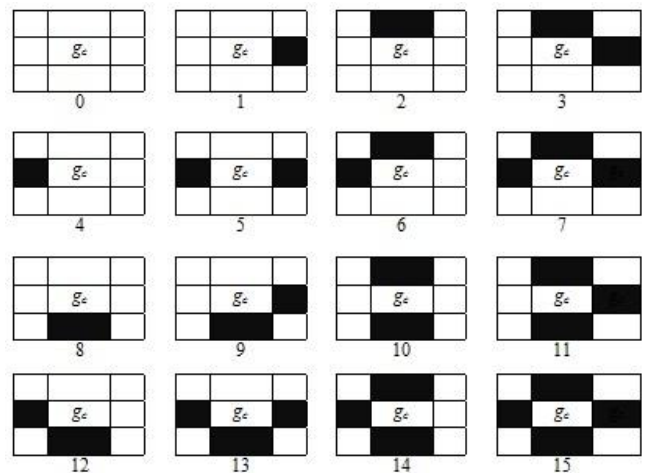


Figure 2. All 16 (2^4) possible patterns generated with $P=4$ and $R=1$.

The presented $LBP_{P,R}^{u2}$ and $LBP_{P,R}^{vu2}$ operators calculate their feature vectors based on the specifics of the pattern, i.e., they are not affected by the grey scale transformation.

Ojala *et al.* [18] provided an alternative description scheme, the variance descriptor ($VAR_{P,R}$ for short). $VAR_{P,R}$ calculates the contrast between the g_c pixel neighbours as shown Figure 1. The $VAR_{P,R}$ operator is rotationally invariant and uses the following formula to calculate the contrast between these neighbours:

$$VAR_{P,R} = \frac{1}{P} \sum_{p=0}^{P-1} (g_p - \mu)^2, \quad \text{where } \mu = \frac{1}{P} \sum_{p=0}^{P-1} g_p \quad (5)$$

Describing an image with $m*n$ pixels using Equation 5 generates an $(m-2)*(n-2)$ output feature vector. In fact, the produced feature vector is not concise and therefore, not practical especially in real-world applications because the longer feature vector has a higher computational cost for the matching process. To reduce the size of the produced feature vector, a quantization operation is needed. Ideally, to maintain statistical stability, the quantization method should produce an average of 10 entries per bin.

3.2. Achieving Shear Invariants

As mentioned above, 2^P different patterns can be generated by employing the $LBP_{P,R}$ code. To investigate the optimal number of neighbours P and radius R to cope with the texture rotation problem, the authors in [7, 27] and many others, experimented with various values of P ($P=4, 8, 12, 16, 24$) and R ($R=1, 2, 3$). They concluded that the best results were obtained with a relatively large number of involved neighbours, like 24, with a large radius, like 3. However, referring to Figure 3, it's could be realized that the problem is different because shear deformation is employed to shift the relevant neighbours' pixels, besides the g_c , horizontally

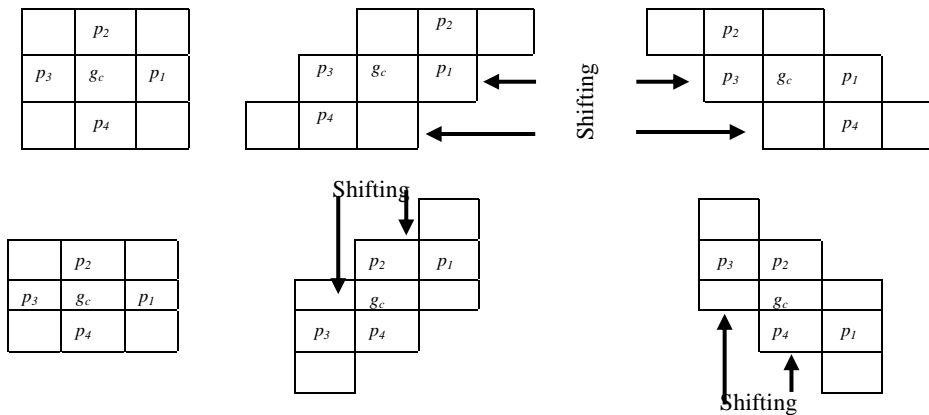


Figure 3. Enlarged 3*3 pattern and its different versions after being deformed with shear: horizontally toward the left, horizontally toward the right, vertically downward, and vertically upward.

3.2.2. Vertical Shear Invariant

To achieve invariant features against vertical shear, a relatively similar method to that provided by the

toward the right or left in the case of horizontal shear (or vertically upward or downward in the case of vertical shear). Therefore, relying on a large P with a large R makes developing a method to extract invariant features extremely difficult, as it's cannot predict the positions of the relevant neighbours of g_c after "shifting" by shear deformation.

Thus, to develop a shear invariant method, we only relied on four neighbours ($P=4$) with radius $R=1$, and based on the type of shear, only two horizontal or vertical neighbours' pixels were involved in extracting the robust features around each g_c pixel.

3.2.1. Horizontal Shear Invariant

To achieve a horizontal shear invariant, a mapping from $LBP_{4,1}$ to $LBP_{4,1}^{hsi}$ (superscript "hsi" denotes horizontal shear invariant) was defined. The $LBP_{4,1}^{hsi}$ mapping has $P(P=4)$ output values (histogram bins) implemented with a 2^P (16) element lookup table $LBP_{4,1}^{hsi}$ is defined as:

$$LBP_{4,1}^{hsi} = \text{sum}(\text{bitget}(LBP_{4,1}, 3) * 2^1, \text{bitget}(LBP_{4,1}, 1) * 2^0) \quad (6)$$

Basically, $\text{bitget}(x, i)$ is used to obtain bit b at position i from the equivalent binary value of x . Then, the summation is obtained by $\text{sum}(b * 2^1, b * 2^0)$. However, in the real world, Equation 6 involves the 1st and 3rd pixels (i.e., p_1 and p_3) around every g_c to achieve the horizontal shear invariant (see the patterns in the first row of Figure 3). In fact, we rely on these two pixels to remove the effect of horizontal shear because their positions are usually invariant with regard to the position of pixel g_c , even though an image transformed by any amount of horizontal shifting, was caused by shear deformation.

$LBP_{4,1}^{hsi}$ method is developed, where a mapping from $LBP_{4,1}$ to $LBP_{4,1}^{vsi}$ (superscript "vsi" denotes vertical

shear invariant) is defined. The defined mapping also has P ($P=4$) output values (histogram bins) implemented with a 2^P (16) element lookup table.

However, the difference lies in the defined formula used to remove the effect of vertical shear deformation.

$LBP_{4,1}^{vsi}$ is defined as:

$$LBP_{4,1}^{vsi} = \text{sum}(\text{bitget}(LBP_{4,1},4)*2^1, \text{bitget}(LBP_{4,1},2)*2^0) \quad (7)$$

Obviously, Equation 7 involves the 2nd and 4th pixels (i.e., p_2 and p_4) around every g_c pixel to achieve the vertical shear invariant. As shown in the patterns of the second row of Figure 3, the positions of these two pixels are usually invariant with respect to the position of pixel g_c , even though an image transformed by any amount of vertical shifting, was caused by shear deformation.

4. First Evaluation

The aim of this evaluation was to apply the proposed shear invariant method to a real-world challenge using texture images obtained from scanned papers. One of the recent relevant active applications in this area is paper fingerprinting. As mentioned previously, all the existing approaches for scanned paper texture fingerprinting have ignored the effect of naturally occurring shear transformations. Therefore, a fingerprinting method that adopts the Shearing Invariant Texture Descriptor (SITD) proposed in this paper is developed to extract unique features.

4.1. Design of Fingerprinting Method

In order to design the paper fingerprinting method, a similar standard architecture to the method proposed in [3] was adopted. Hence, the developed scanned paper texture fingerprinting method is composed of two stages, namely, fingerprint generation (registering) and fingerprint validation. Both are shown in Figure 4.

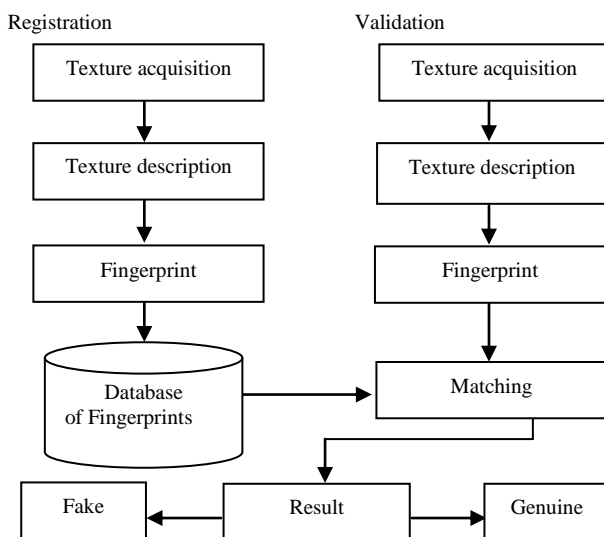


Figure 4. Proposed stages of the fingerprinting method.

4.1.1. Fingerprint Generation (Registration)

The first stage involves obtaining a unique fingerprint from the document texture. The fingerprint can be printed on the physical paper itself for future verification or stored in a database. Generating the fingerprint involves the following two steps:

- *Texture Acquisition:* In the first step, the texture of the document surface is acquired using a commodity desktop scanner. Developing a paper texture fingerprinting method that adopts a non-movable sensor instead of a movable sensor provides a low-cost technique with easy-to-use features.
- *Feature Extraction:* In this step, the obtained texture image is converted into a robust, unique, and concise feature vector using the proposed SITD. Each texture image is described with a four bin histogram. The obtained feature vector is considered as a texture fingerprint.

4.1.2. Fingerprint Validation

The validation process is quite similar to the fingerprint generation one as shown in Figure 4, in that a new paper texture is acquired and the feature vector calculated. The only difference in this stage is the feature (fingerprint) matching. The validation process is employed to evaluate the goodness between two fingerprints obtained from the two stages of the developed fingerprinting method. To evaluate the goodness between fingerprints, the chi-squared distance which given by the following equation is used:

$$\chi^2(M, S) = \sum_{i=1}^N (M_i - S_i)^2 / S_i \quad (8)$$

Where N represents the number of bins and M_i and S_i are the values of bin i in the model and sample fingerprints, respectively.

4.2. Data Collection and Experiment

A texture image dataset was collected from the surfaces of white A4 blank papers. The dataset consisted of three main sets with the only difference between these sets being the acquisition resolution. The following resolutions were adopted: 50 dpi, 100 dpi, and 150 dpi for the first, second, and third sets, respectively. The sizes of the images in these sets were 425*585 pixels, 850*1169 pixels, and 1275*1754 pixels, respectively. Each of the three sets included 102 texture images. The images in the second set were obtained from the work presented in [14]. The collected image dataset is available at the official website of the Pattern Recognition research group-National University of Malaysia [16].

The texture images in all three sets were acquired using a desktop Epson GT-2500 scanner. To obtain

the 102 texture images in each set, 51 papers were scanned twice. For the first scan, the papers were in the ideal scanning position (i.e., with 0° rotation), while for the second scan, the papers were rotated based on a corner pivot of roughly 2° to generate the shear deformation. Figure 5 shows the texture acquisition process from blank paper in both the ideal and rotated positions.

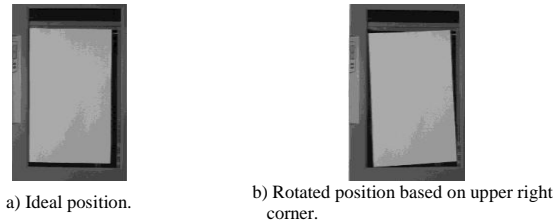


Figure 5. Image acquisition.

In each set, the data were equally divided into test and reference datasets. The original (undistorted) images were used as reference data, while the rest were used as test data.

To obtain fingerprints from a texture image, four representative disjoint sub-image patches, with size 50×50 pixels, were used. These patches were placed at the image corners, with the centres of the square patches 125×125 pixels away from the image corners. However, to ensure that these patches were obtained from the correct positions, four registration marks were fixed on the physical paper to identify the centres.

Later, the proposed shear invariant descriptor was applied to each obtained patch and the extracted features from the four patches were merged. The merged feature vectors were considered as a ‘‘paper fingerprint’’.

Finally, the chi-square test was employed to calculate the dissimilarity degree between features extracted from the test and reference data. Therefore, fingerprints with the least dissimilarity were considered to be identical.

For the purpose of performance comparison, the SMI descriptor and the conventional Rot-LBP including $LBP_{P,R}^{u,2}$, $LBP_{P,R}^{v,2}$, and $VAR_{P,R}$ as well as the joint distribution between $LBP_{P,R}^{u,2}$ and $VAR_{P,R}$ ($LBP_{P,R}^{u,2}, VAR_{P,R}$), were applied to the image dataset in a similar manner to that explained above. The features obtained from the $VAR_{P,R}$ operator were quantized to achieve stability from a statistical perspective as described in [18]. As a result, each bin in the feature vector included an average of 10 entries. To the best of our knowledge, for the Rot-LBP operators, various values of P and R were tested.

4.3. Results

The experimental setup is implemented for the developed texture dataset by obtaining four patches

from each texture image with the help of registration marks. In the description stage, applying the proposed shear invariant method to the sub-image patch produced a histogram with four bins, whereas merging the histograms obtained from the four patches generated a 16-bin histogram representing the unique image texture fingerprint. Table 1 presents the number of bins in the histogram produced by applying each of the proposed shear descriptor operators, as well as the SMI and different operators of Rot-LBP, to a single patch.

In Table 1, the purity percentages of correct authentication to the test papers are presented as the first choice. The results under the columns labelled 50, 100, and 150 refer to the performance of the proposed descriptor as well as benchmark methods to texture images from the first, second, and third sets, respectively, from the developed dataset.

Several findings are observed from Table 1. First, as expected, the proposed $LBP_{4,1}^{hsi}$ outperformed the $LBP_{4,1}^{vsi}$ because horizontal shear is the dominant transformation as proved in the simulation presented in [14] and utilized images similar to those used in the current experiment. We are of the opinion that the $LBP_{4,1}^{vsi}$ could produce similar excellent results to those for $LBP_{4,1}^{hsi}$ if it’s used in areas where the dominant shear transform is along the vertical axis.

Second, the proposed horizontal shear invariant $LBP_{4,1}^{hsi}$ achieved perfect performance with a resolution of 100 dpi and above; all the papers were authenticated correctly, i.e., the performance accuracy was 100%. This demonstrates the efficiency and stability of relying on two horizontal neighbouring pixels to the centre pixel of the local pattern. However, as expected, the performance of the proposed descriptor in the first set, which included images acquired with 50 dpi resolution, was not as good as the other test sets. The percentage of correctly authenticated documents was 68.6%, meaning that 70/102 papers were authenticated correctly. This result was achieved because the amount of information acquired under this resolution is relatively low, thus challenging the image descriptor method.

Third, the proposed $LBP_{4,1}^{hsi}$ placed the SMI and Rot-LBP as viable alternatives in terms of performance accuracy. The SMI in the best case correctly authenticated 79 of the 102 tested papers (in the third test set). However, this is not acceptable in critical applications such as paper fingerprinting. For the $LBP_{P,R}^{u,2}$ and $LBP_{P,R}^{v,2}$ operators, the best results were usually obtained with a small radius, i.e., $R=1$, and this extended to the merged operators where $R=1$. That is because the positions of the nearest pixels and their grey values are least affected by the shear

transformation compared with relatively far pixels when $R=2$ or 3. However, the worst performance among these operators shown by rotation invariant variance ($VAR_{P,R}$). That is attributed to the grey-scale variance created by shear transformation. The performance of $VAR_{P,R}$ was slightly enhanced after calculating the joint distribution with its complement from $LBP_{P,R}^{riu2}$, i.e., $LBP_{P,R}^{riu2} / VAR_{P,R}$.

Table 1. Performance rate (%) for paper texture fingerprinting.

Operator	P,R	Bins	Resolution (DPI)		
			50	100	150
$LBP_{P,R}^{hsi}$	4,1	4	68.6	100	100
$LBP_{P,R}^{vsi}$	4,1	4	37.3	43.1	45.1
$LBP_{P,R}^{u2}$	4,1	15	66.7	78.4	85.2
	8,1	59	43.1	45.1	64.6
	12,2	135	56.9	58.8	62.7
	24,3	555	35.3	45.1	52.9
	4,1+8,1	15+59	54.9	60.8	78.4
	4,1+12,2	15+135	60.8	62.7	78.4
	4,1+24,3	15+555	56.9	60.8	70.5
	8,1+12,2	59+135	60.7	66.7	70.6
	8,1+24,3	59+555	56.8	56.8	60.8
	12,2+24,3	135+555	52.9	60.8	72.5
	4,1+8,1+ 12,2+24,3	15+59+ 135+555	60.8	70.5	74.5
	$LBP_{P,R}^{riu2}$	4,1	6	50.9	50.9
8,1		10	50.9	60.8	52.9
12,2		14	35.3	37.2	37.3
24,3		26	29.4	45.1	52.9
4,1+8,1		6+10	39.2	43.1	58.8
4,1+12,2		6+14	47.1	47.1	49
4,1+24,3		6+26	27.4	56.8	64.7
8,1+12,2		10+14	41.1	47.1	50.9
8,1+24,3		10+26	35.2	37.3	58.8
12,2+24,3		14+26	45	54.9	56.9
4,1+8,1+ 12,2+24,3		6+10+ 14+26	47.1	54.9	64.7
$VAR_{P,R}$		4,1	230	3.9	5.8
	8,1	230	1.9	5.8	7.8
	12,2	230	1.9	7.8	13.7
	24,3	230	1.9	5.8	11.8
	4,1+8,1	230+230	1.9	1.9	5.9
	4,1+12,2	230+230	1.9	5.8	9.8
	4,1+24,3	230+230	1.9	3.9	17.6
	8,1+12,2	230+230	1.9	7.8	13.7
	8,1+24,3	230+230	1.9	1.9	21.6
	12,2+24,3	230+230	1.9	7.8	15.7
	4,1+8,1+ 12,2+24,3	230+230+ 230+230	1.9	3.9	11.8
	$LBP_{P,R}^{riu2} / VAR_{P,R}$	4,1	6/230	54.9	50.9
8,1		10/230	35.2	56.9	58.8
12,2		14/230	37.3	37.3	39.2
24,3		26/230	29.4	49.1	52.9
4,1+8,1		6/230+10/230	37.2	37.3	62.7
4,1+12,2		6/230+14/230	39.2	43.1	47.1
4,1+24,3		6/230+26/230	27.4	37.2	49
8,1+12,2		10/230+14/230	39.2	39.2	47.1
8,1+24,3		10/230+26/230	47.1	49	45
12,2+24,3		14/230+26/230	43.2	41.1	54.9
4,1+8,1+ 12,2+24,3		6/230+10/230+ 14/230+26/230	47	52.9	54.9
<i>SMI</i>		-	7	60.7	68.6

Fourth, as with the proposed description method, the benchmark methods usually showed better performance for images acquired with 100 dpi resolution and above.

Finally, the proposed descriptor produced a vector with only four bins as a description for each sub-image compared with 6 bins and 15 bins from $LBP_{P,R}^{riu2}$ and

$LBP_{P,R}^{u2}$, respectively (with $P=1$), and seven bins from *SMI*. In fact, this is an additional advantage of the

proposed descriptor, especially in online applications, because a smaller number of bins in the feature vector require lower computational cost for feature matching.

5. Second Evaluation

In this evaluation, the performance of the proposed description method was evaluated on two different shear deformation problems. The images used in both experiments were sheared artificially by software.

Therefore, the problems were slightly simplified compared with the challenge presented in the first evaluation, and at the same time, they were highly controlled.

5.1. First Experiment

The primary objective of this experiment was to demonstrate the performance of the proposed method on standard images obtained from a wide spectrum of surface textures of artificial and natural materials. Therefore, the state-of-the-art Outex texture dataset is selected to achieve this purpose.

5.1.1. Image Dataset and Experimental Setup

All 320 original (undistorted) texture surface images available in the current Outex dataset were used. Each image was sheared with five different shearing factors (2, 7, 15, 30, and 60) along the horizontal-axis. Figure 6 shows the original images and the corresponding sheared images. Then, the images sheared with the same factor together with the original images were stored in separate sets. In total, a dataset consisting of 3200 texture images is obtained. The dataset was divided into five testing sets, with each set comprising 640 texture images.

As in the first evaluation, the data in each set were equally divided into test and reference data. The original images were used as the reference data with the remaining images used as test data. Later, the proposed descriptor was employed to extract features from whole images. Finally, the chi-square test was used to calculate the dissimilarity between the extracted features from both the test and reference images.

5.1.2. Experimental Results

The results of this experiment are presented in Table 2. As in Table 1, these results represent the purity percentages of correctly recognized textures as the first choice. The obtained results show the excellent performance and stability of the proposed method regardless of the amount of shear transform. This reveals the efficiency of the adopted strategy of relying on two neighbouring pixels.

Table 2. Correctly recognized images (%) versus different amounts of shearing.

Operator	P,R	Shearing in x-direction				
		2	7	15	30	60
$LBP_{P,R}^{hsi}$	4,1	100	100	100	100	100
$LBP_{P,R}^{vsi}$	4,1	72.5	56.5	42.8	29.4	24.1
$LBP_{P,R}^{u2}$	4,1	58.4	50.6	44.1	30.3	16.6
	8,1	84.4	82.2	79.7	71.3	59.1
	12,2	87.2	85	82.8	73.4	63.8
	24,3	62.8	64.4	63.8	66.6	67.8
	4,1+8,1	86.6	82.5	77.8	67.8	57.5
	4,1+12,2	69.5	84.1	79.4	69.4	60.3
	4,1+24,3	81.9	78.1	75.3	65.6	56.6
	8,1+12,2	88.4	87.2	83.7	74.7	67.5
	8,1+24,3	88.1	87.5	85.6	80.9	75.9
	12,2+24,3	88.7	87.5	86.3	80.9	75.3
	4,1+8,1+12,2+24,3	87.8	86.6	83.7	74.4	67.5
	$LBP_{P,R}^{riu2}$	4,1	34.4	30.4	26.2	12.5
8,1		59.1	58.6	54.6	42.2	43.7
12,2		62.6	60.1	58.7	46.9	44.6
24,3		72.8	71.4	67.7	56.6	56.8
4,1+8,1		81.3	79.5	74.9	61.6	61.8
4,1+12,2		83.1	79.5	76.8	62.8	62.8
4,1+24,3		86.2	84.8	80.5	65.9	66.1
8,1+12,2		81.2	80.1	77.4	62.2	62.1
8,1+24,3		84.4	83.6	80.8	67.5	66.5
12,2+24,3		86.2	84.8	80.6	67.2	65.2
4,1+8,1+12,2+24,3		85.6	82.9	80.2	65.3	66.2
$VAR_{P,R}$		4,1	13.4	11	10.3	7.2
	8,1	86.6	84.1	81.9	85	82
	12,2	83.7	83.2	85	85.3	81.4
	24,3	84.4	81	81.2	82.1	76.1
	4,1+8,1	17.8	14.1	14.7	11.3	13.6
	4,1+12,2	17.8	14.4	14.7	11.3	13.3
	4,1+24,3	17.8	14.4	14.7	11.3	13.5
	8,1+12,2	85.3	84.4	84.1	86.3	80.8
	8,1+24,3	85.6	84.1	82.5	86.2	79.8
	12,2+24,3	84.7	82.9	82.2	84.7	79.5
	4,1+8,1+12,2+24,3	23.1	22.3	18.8	N/A	N/A
	$LBP_{P,R}^{riu2} / VAR_{P,R}$	4,1	13.1	11.2	10.9	8.8
8,1		90.9	92.5	94.7	94.7	90.6
12,2		90.3	94.1	95.6	95.3	92.8
24,3		95	94.3	94.7	96.2	93.4
4,1+8,1		18.8	16.3	20.3	15.3	15.6
4,1+12,2		19.1	16.6	20.6	15.9	15.6
4,1+24,3		18.4	17.2	20.6	15.9	15.9
8,1+12,2		94.1	93.8	95.3	95	90.9
8,1+24,3		94.3	94.1	95	96.3	92.6
12,2+24,3		95.6	94.7	95.3	95.3	92.8
4,1+8,1+12,2+24,3	N/A	N/A	N/A	N/A	N/A	
SMI	-	71.3	37.5	18.7	6.2	3.1

In fact, even if the amount of shear transform is greater than the values tested in this experiment, we are confident that the correct information could still be retrieved. The largest shearing amount tested in this experiment (equal to 60), which is considered high, is shown in Figure 6-f.

The results of the benchmark methods are logical, with the amount of shear transform inversely proportional to performance. However, the performance of the benchmark methods is better than that reported in previous experiments owing to the texture materials used in this experiment; recognizing a texture dataset that includes a variety of materials is considerably easier than recognizing a texture dataset collected from a single material.

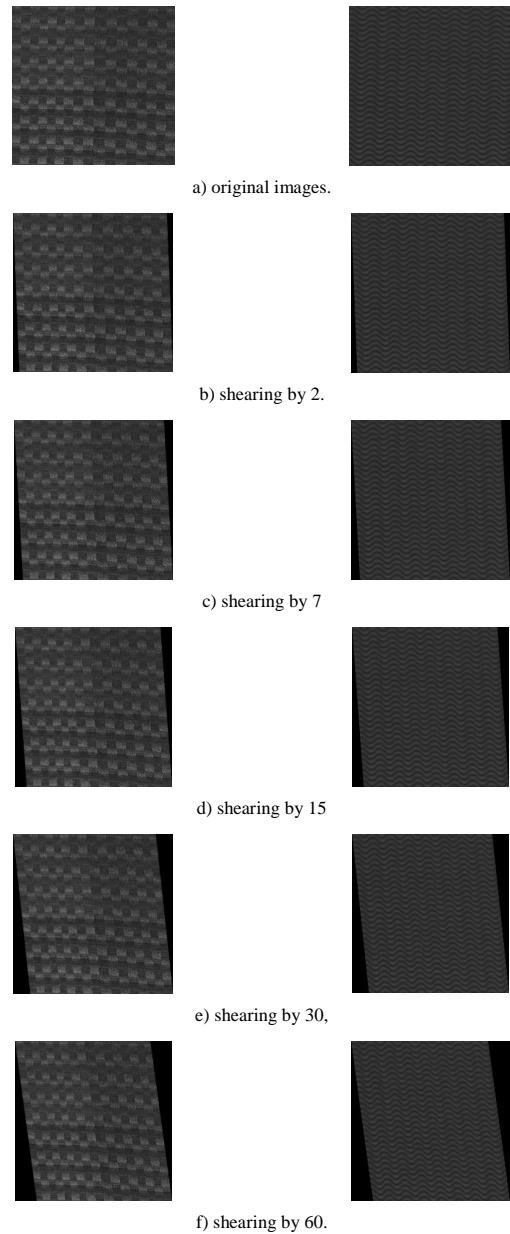


Figure 6. Samples of original textures from Outex and the corresponding sheared images.

5.2. Second Experiment

The final experiment conducted on standard images included distinctive shapes rather than textures. This experiment was quite interesting as it's provided an evaluation of the shearing invariant descriptor proposed in this paper to shape-based image recognition. As with texture-based recognition, shape-based recognition also has a variety of applications that include shearing variation, especially when scanners are used to acquire the images.

The experiment conducted in [14] is replicated with the current experiment, whereas they used 12 standard images (Barbara, Cameraman, Fingerprint, Flintstones, House, and Lena plus the corresponding sheared images). Figure 7 shows the images used in the experiment. In the experimental setup, the original images were used as reference data and the distorted images as test data. In fact, the sheared versions of

those images were obtained by shearing the original images artificially by software. Moreover, the performance results of SMI reported in [14] were used in comparison to those collected from the proposed descriptor.



Figure 7. Original images (upper row) and the corresponding sheared images (lower row) for (from left to right) Barbara, Cameraman, Fingerprint, Flintstones, House, and Lena.

5.2.1. Obtained Results

Both reference and test data were described with the proposed feature descriptor. Later, the dissimilarity degrees between the extracted features from the reference and test data are calculated. The obtained results are listed in Table 3, where the columns represent the reference data and the rows the test data.

The results presented in Table 3 show that the degree of dissimilarity between each original image and its corresponding sheared image is the lowest compared with the other sheared images. This means that all the images were recognized correctly and retrieved as a first choice. Comparing these results with the corresponding results obtained using the SMI descriptor demonstrates the superiority of the proposed method. As reported in [14], the SMI descriptor recognized only four of the six tested images, while the remaining two images (Flintstones and Lena) were recognized only as a third choice.

Table 3. Dissimilarity degrees between original (undistorted) images (column headings) and shear images (italicized row labels).

Images	Barbara	Cameraman	Fingerprint	Flintstones	House	Lena
Barbara	82.4	3266.9	1100.9	252.7	746.9	524.9
Cameraman	1657.8	220.1	5884.9	1368.1	330.6	3725.2
Fingerprint	1522.1	7967.7	34.4	1992.6	3726.7	843.4
Flintstones	117.2	2821.1	1469.5	75.7	613.4	432.9
House	468.2	1905.6	2841.8	473.9	190.5	1280.1
Lena	1345.4	6572.9	1022.01	1436.4	2.7123	97.1

6. Conclusions

In this paper, a new SITD based on rotation invariant LBP descriptor was presented. Two operators, $LBP_{4,1}^{hsi}$ and $LBP_{4,1}^{vsi}$, were defined to achieve either horizontal or vertical shearing invariant features. Both were relied on four neighbours ($P=4$) with radius $R=1$ in the images local patterns. The superior performance of the proposed descriptor was demonstrated with various challenged experiments, whereas the $LBP_{4,1}^{hsi}$ operator achieved up to 100% in all the experiments. Also, the proposed descriptor obtained much better accuracy results than the state-of-the-art conventional rotation invariant LBP and the SITDs.

The efficient performance of the proposed descriptor could be benefit in different real-world applications. Possible applications include offline character recognition, digit recognition, old manuscript restoration, and document retrieval. The proposed descriptor can also be used to tackle shear deformation produced in Computed Tomography (CT) images. As Hill *et al.* [9] stated, shear deformation is the most common distortion in CT images and is produced when a tilted CT gantry rotates the image plane with respect to the axis of the bed. Another application that may benefit from the descriptor is remote sensing systems where skew (shear) distortion is common in imagery obtained from satellite multispectral scanners [20].

Acknowledgments

This work was funded by Department of Higher Education of Malaysia with research grant FRGS-1-2012-SG05-UKM-02-02.

References

- [1] Abbadeni N., "Texture Representation And Retrieval Using The Causal Autoregressive Model," *Journal of Visual Communication and Image Representation*, vol. 21, no. 7, pp. 651-664, 2010.
- [2] Buchanan D., Cowburn P., Jausovec V., Petit D., Seem P., Xiong G., Atkinson D., Fenton K., Allwood A., and Bryan M., "Forgery: Fingerprinting Documents and Packaging," *Nature*, pp. 436-475, 2007.
- [3] Clarkson W., Weyrich T., Finkelstein A., Heninger N., Halderman A., and Felten E., "Fingerprinting Blank Paper Using Commodity Scanners," in *Proceeding of 30th IEEE Symposium on Security and Privacy*, California, pp. 301-314, 2009.
- [4] Garain U. and Halder B., "On Automatic Authenticity Verification Of Printed Security Documents," in *Proceeding of the 6th Indian Conference on Computer Vision, Graphics, and*

- Image Processing*, Bhubaneswar, pp. 706-713, 2008.
- [5] Gehrke R. and Greiwe A., "Multispectral Image Capturing with Foveon Sensors," in *Proceeding of International Archives of the Photogrammetry, Remote Sensing and Spatial Information Sciences*, Rostock, pp. 151-156, 2013.
- [6] Guo K., Labate D., Lim W., Weiss G., and Wilson E., "Wavelets with Composite Dilations," *Electronic research Announcements of the American Mathematical Society*, vol. 10, no. 9, pp. 78-87, 2004.
- [7] Guo Z., Zhang L., and Zhang D., "A Completed Modelling Of Local Binary Pattern Operator For Texture Classification," *IEEE Transactions on Image Processing*, vol. 19, no. 6, pp. 1657-1663, 2010.
- [8] Han R. and Zhang L., "Fabric Defect Detection Method Based on Gabor Filter Mask," in *Proceeding of IEEE Global Congress on Intelligent Systems*, Washington, pp. 184-188, 2009.
- [9] Hill D., Batchelor P., Holden M., and Hawkes D., "Medical Image Registration," *Physics in Medicine and Biology*, vol. 46, no. 3, pp.1-45, 2001.
- [10] Kenzel W., Rothermel M., Fritsch D. and Haala N., "Image Acquisition and Model Selection for Multi-View Stereo," *The International Archives of the Photogrammetry, Remote Sensing and Spatial Information Sciences*, Stuttgart, pp.251-258, 2013.
- [11] Kiertscher T., Fischer R., and Vielhauer, C., "Latent Fingerprint Detection Using A Spectral Texture Feature," in *Proceeding of the 13th ACM Workshop on Multimedia and Security*, New York, pp. 27-32, 2011.
- [12] Malik F. and Baharudin B., "The Statistical Quantized Histogram Texture Features Analysis for Image Retrieval Based on Median and Laplacian Filters in the DCT Domain," *The International Arab Journal of Information Technology*, vol. 10, no. 6, pp. 616-624, 2013.
- [13] Metois E., Yarin P., Salzman N., and Smith R., "Fiber Fingerprint Identification," in *Proceeding of 3rd Workshop on Automatic Identification*, New York, pp. 147-154, 2002.
- [14] Nasrudin M., Wahdan O., and Omar K., "Irregular Rotation Deformation from Paper Scanning: An investigation," in *Proceeding of the International Neural Network Society Winter Conference*, Bangkok, pp. 152-161, 2012.
- [15] Nordin M. and Abdul-Hamid A., "Combining Local Binary Pattern and Principal Component Analysis on T-Zone Face Area for Face Recognition," in *Proceeding of International Conference on Pattern Analysis and Intelligent Robotics*, Kuala Lumpur, pp. 25-30, 2011.
- [16] Official Website Of The Pattern Recognition Research Group-National University of Malaysia <http://www.ftsm.ukm.my/pr/>, Last Visited 2014.
- [17] Ojala T., Maenpaa T., Pietikainen M., Viertola J., Kyllönen J., and Huovinen S., "Outex-New Framework For Empirical Evaluation of Texture Analysis Algorithms," in *Proceeding of 16th International Conference on Pattern Recognition*, Quebec, pp. 701-706, 2002.
- [18] Ojala T., Pietikainen M., and Maenpaa T., "Multiresolution Gray-Scale and Rotation Invariant Texture Classification with Local Binary Patterns," *IEEE Transactions on Pattern Analysis and Machine Intelligence*, vol. 24, no. 7, pp. 971-987, 2002.
- [19] Petrou M. and Sevilla P., *Image Processing: Dealing with Texture*, Wiley, 2006.
- [20] Richards J., *Remote Sensing Digital Image Analysis*, Springer, 2012.
- [21] Shamsuddin M., "Higher Order Centralized Scale-Invariants for Unconstrained Isolated Handwritten Digits," *PhD Thesis*, Universiti Putra Malaysia, Malaysia, 2000.
- [22] Vácha P., Haindl M., and Suk T., "Colour and Rotation Invariant Textural Features Based on Markov Random Fields," *Pattern Recognition Letters*, vol. 32, no. 6, pp. 771-779, 2011.
- [23] Varma M. and Zisserman A., "A Statistical Approach to Material Classification Using Image Patch Exemplars," *IEEE Transactions on Pattern Analysis and Machine Intelligence*, vol. 31, no. 11, pp. 2032-2047, 2009.
- [24] Vera D., "Shear Anisotropic Inhomogeneous Besov Spaces in RD," *International Journal of Wavelets, Multiresolution and Information Processing*, vol. 12, no. 1, 2014.
- [25] Wahdan O., Nasrudin M., and Omar K., "SITD and Across-Bin Matching for Deformed Images Acquired by Scanners," in *Proceeding of IEEE 10th International Colloquium on Signal Processing and its Applications*, Kuala Lumpur, pp. 14-19, 2014.
- [26] Wang Z. and Yong H., "Texture Analysis And Classification With Linear Regression Model Based On Wavelet Transform," *IEEE Transactions on Image Processing*, vol. 17, no. 8, pp. 1421-1430, 2008.
- [27] Wei H., Zhu H., Gan Y., and Shang L., "A New LBP in Texture Classification," in *Proceeding of 10th International Conference on Intelligent Computing*, Taiyuan, pp. 700-705, 2014.
- [28] Zhu B., Wu J., and Kankanhalli M., "Print Signatures For Document Authentication," in *Proceeding of 10th ACM Conference on Computer and Communications Security*, Washington, pp. 145-154, 2003.
- [29] Žunić J., Hirota K., and Rosin L., "A Hu Moment Invariant as A Shape Circularity

Measure,” *Pattern Recognition*, vol. 43, no. 1, pp. 47-57, 2010.



Omar Wahdan Received the B.Sc. (2008) in computer science from the University of Baghdad and M.Sc. (2011) in Artificial Intelligence from the Universiti Kebangsaan Malaysia (UKM). Currently, he pursues his Ph.D. in the field of texture authentication at the Faculty of

Information Science and Technology-UKM. He is also Graduate Research Assistant at the same Faculty. His research interest includes pattern recognition applications where he has authored several publications in this area.



Mohammad Nasrudin is an active researcher at the Centre for Artificial Intelligence Technology (CAIT), UKM. He obtained his B. of Business Administration degree majoring in Computer Information System at the Western Michigan

University. He received a master's from Universiti Kebangsaan Malaysia (UKM) and a Ph.D. in AI by joining the Malaysia-Imperial College Doctoral Programme. Mohammad's doctoral thesis was a study of image feature construction using the Trace transform, which was guided by the late Prof. Maria Petrou. His current research focuses on document analysis and recognition and metaheuristic optimization.



Khairuddin Omar Received his BSc and M.Sc. in Computer Science from Universiti Kebangsaan Malaysia (UKM) in 1986 and 1989, respectively, and Ph.D. in 2000 from Universiti Putra Malaysia. Currently, he is a Professor at the Faculty of

Information Science and Technology, UKM. His research interests includes AI, pattern recognition in decision making with uncertainty-Bayesian Reasoning, Neural Networks, Fuzzy Logic, Fuzzy Neural Networks, 2D and 3D image processing, edge detection, thinning, segmentation, feature extraction, texture, resolution, Fourier, Wavelet, etc., with applications to Jawi/Arabic Manuscripts, biometric authentication.